

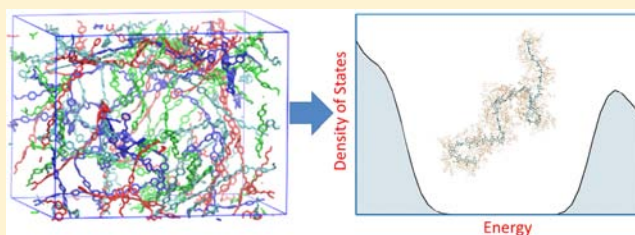
Relation between Structure and Electronic Properties of Amorphous MEH-PPV Polymers

Ting Qin and Alessandro Troisi*

Department of Chemistry and Centre of Scientific Computing, University of Warwick, CV4 7AL Coventry, United Kingdom

S Supporting Information

ABSTRACT: Classical molecular dynamics simulations were used to build several large models of the amorphous polymeric semiconductor MEH-PPV. A balanced set of approximations was determined to evaluate the electronic structure of these large systems, providing quantitative information for the understanding of the charge transport properties. We have verified that the electronic structure is largely determined by the conformational disorder of the individual chains, with little effect of electrostatic disorder and interchain coupling. The disorder is essentially static, although thermal motions cause an evolution of the single chain orbital energies. The localization length of the orbitals relevant for transport is energy-dependent, unlike what is normally assumed in variable range hopping methods. Although we have found evidence of correlation between planarity of the polymer chain and localization of the highest valence band orbitals, the correlation is moderate and exceptions are frequent. All observations are discussed in terms of the desirable characteristics that should be included in a model of transport for amorphous polymeric semiconductors.



■ INTRODUCTION

The qualitative features of charge transport in polymeric semiconductors seem to be clear,^{1–5} but it is still very difficult to establish a correlation between chemical structures and charge transport properties of these materials. It was believed for many years that increased local order was the key ingredient for high charge mobility,^{6,7} but the introduction of new high-mobility amorphous polymers^{8,9} indicates that we have not identified clearly all the elements that make a good polymeric semiconductor.

It seems well-established that the charge transport in an amorphous material can be described as a series of incoherent hopping events. The states are localized by the electrostatic or conformational disorder of the polymer and can be further localized by charge-phonon coupling.^{10,11} Phenomenological models of transport can be constructed by making hypotheses on the shape of the density of states (DOS) and the hopping rate between states.¹ The latter is influenced by the localization length of the charges and determines the type of variable range hopping methods used.¹² These methods can describe the electrical characteristics of the device, but they are too coarse to provide information on the desirable chemical characteristics of a polymer or the chemical nature of trap states for the carrier. Electronic structure calculations based on realistic polymer conformation show that the shape of the DOS cannot be assumed to be a simple function (typically a Gaussian) and that the hopping rate is dependent on the energy of the carrier with higher energy carriers being able to hop at longer distances.⁶

Going beyond phenomenological models requires the construction of an atomistic model of the polymer and the evaluation of its electronic structure. Both tasks are particularly

challenging from the computational point of view, and the majority of papers have focused only on one of them at a time. In this paper, we consider one of the prototypical amorphous polymers, the soluble poly(phenylenevinylene) (PPV) derivative MEH-PPV^{13–15} (see Figure 1a), and we perform an evaluation of its microscopic structure in bulk, the DOS, the localization length, and the correlation between electronic and structural features. We present a methodology that can be used for any polymer and may form the basis to establish more rigorously the structure–property relation in these materials.

Several classical simulation studies of PPV derivatives have appeared in the literature. PCFF force field¹⁶ was applied to a bulk MEH-PPV system containing three 10 monomer chains,¹⁷ a length that is too short to correctly evaluate the localization length of charge carrier states on the chain (as we will see). The MM3 potential was used to simulate a single MEH-PPV chain in solvent,¹⁸ but it is expected that the distribution of conformations accessible in the bulk is different than that in the solvent. Coarse grain potentials can also be applied to describe the chain morphology of this class of polymers,^{19–22} but they do not contain enough information to construct the electronic wave function. The challenge for the classical atomistic simulation of bulk amorphous polymer is in the large size of the system and the nontrivial force fields that are needed by conjugated polymers, as highlighted in the works of Raos^{23,24} and Friesner's^{25,26} groups. In a recent paper, one of these specialized force fields²⁶ was applied to bulk MEH-PPV,

Received: May 2, 2013

Published: July 8, 2013

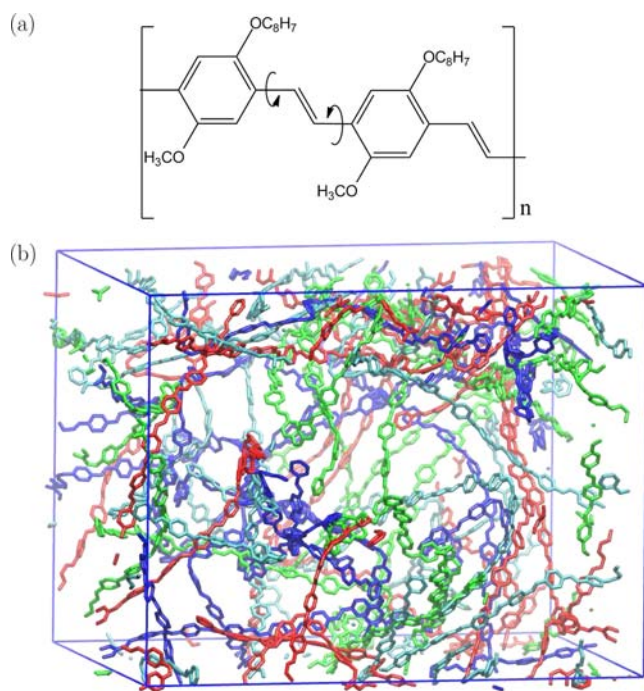


Figure 1. (a) Structure of MEH-PPV polymer (two monomers shown) with the curved arrows indicating the torsion angles ψ_1 and ψ_2 used in the conformational analysis. (b) Structure of m40t20 system at 200 ns with cell size of $59 \times 59 \times 77$ Å. In total, 16 chains are illustrated in 4 different colors, and only backbone carbon atoms are shown.

but the analysis was carried out only on the geometric structure of the model.

The electronic structure calculation of large models of amorphous polymer is naturally very demanding as there is no translational symmetry that can be used to reduce the size of the problem. The situation is more approachable for semi-crystalline polymers for which it is possible to study the electronic structure of one lamella at a time, reducing drastically the number of atoms of the system.^{6,27,28} All attempts have to rely on some level of approximations to bring the computational cost to an acceptable level, considering that such calculations need to be repeated a number of times to provide representative averages of the material properties. For example, McMahon et al. proposed an ad hoc linear-scaling tight-binding method for rapid calculations of large polymers based on the partitioning of the system into its monomeric components.²⁸ Vukmirović et al. developed a charge patching method (CPM) which approximates the electronic charge density of the large system by simply adding the contributions of individual atoms.²⁹ They also designed an overlapping fragments method³⁰ for the diagonalization of a single-particle Hamiltonian obtained from the CPM³¹ and applied this methodology to large-scale polymer systems.³² Recently, they developed a nearest-neighbor tight-binding model with a correlated Gaussian distribution of on-site energies for large-scale system calculations.³³ Semiempirical methods are also very frequently used, in particular, for the study of excited-state properties.^{34–36} In addition to these methods, fragment molecular orbital method and the alternative localized molecular orbital method³⁷ have been used for a range of large systems from DNA³⁷ to polymers.³⁸

In this paper, we will first construct a reliable force field for MEH-PPV and provide its validation. We will then use molecular dynamics (MD) to generate several large-scale models of MEH-PPV. These models will be used as the input for large-scale electronic structure calculations based on a divide and conquer method that we present and validate here, as well. We will analyze the results primarily in terms of DOS and localization length of the system orbitals. We will also correlate the localization of the orbital with the structural features that in the literature are traditionally believed to be responsible of charge trapping in PPV, namely, the tetragonal defects¹⁵ and the local planarity.⁶

METHODS

The C–C bonds along the backbone of MEH-PPV have different equilibrium lengths, depending on the different bond order between nonequivalent pairs of sp^2 carbon atoms. The potential for the torsion about these bonds is also a function of the bond order, and for this reason, it is imperative to consider a force field that differentiates between the different types of $C_{sp^2}-C_{sp^2}$ bonds present in this system. The MM3 force field was specifically designed to model π -conjugated systems taking into account the variation of the bond order among different atoms.^{26,39–41} Within the MM3 force field, a self-consistent field Pariser–Parr–Pople (PPP)-type calculation was first carried out on the π system to obtain the bond orders, and the bond length, natural bond strength constant, and the second-order torsion constant are linearly related to the bond order.

Several aspects of the MM3 force field are, however, unsuitable for software specialized for simulation of very large systems (e.g., usage of dipole instead of point charge electrostatics), and for this reason, we adopted Raos' procedure^{23,42} to convert the MM3 functional form to an OPLS functional form,⁴³ a procedure that proved to work well for small oligomers. Recently, the same procedure has been used to simulate conjugated polymer chains, such as P3HT and PPV systems.²⁶ In this OPLS force field, the atomic point charges are calculated from density functional theory (DFT) calculations; the intramolecular stretching, bending, and torsion terms are transformed from the MM3 force field taking into account bond orders for the $C_{sp^2}-C_{sp^2}$ bonds, and the van der Waals terms take the Buckingham functional form. One parameter in the attractive part of the Buckingham potential was adjusted to reproduce the experimental crystal structure densities, which is the only adjustable parameter within the whole potential construction procedure. Details of the conversion from MM3 force field to OPLS force field are given in the Supporting Information together with a validation of the force field based on the calculation of small oligomers of PPV with known crystal structures.

MD simulations are used to generate several models of MEH-PPV bulk polymer. We started with a completely arbitrary low-density arrangement of the chains, performed an initial high-temperature equilibration at 1000 K, followed by a slow simulated annealing to 300 K and by production dynamics at 300 K. The results of three different simulations will be presented and indicated as m40t20 (40 monomer chain; 20 ns high-temperature equilibration followed by 20 ns of annealing), m40t15 (40 monomer chain; 15 ns high-temperature equilibration followed by 15 ns of annealing), and m20t15 (20 monomer chain; 15 ns high-temperature equilibration followed by 15 ns of annealing). Each system consists of 16 chains.

MD was carried out in the NPT ensemble with the pressure set at 1 atm. The temperature and pressure were controlled using a Nosé–Hoover thermostat and (anisotropic) barostat, respectively. Non-bonded interactions were truncated using a cutoff of 9 Å, and the electrostatics were treated using the particle–particle–mesh Ewald algorithm with a precision of 10^{-4} . The equations of motion were integrated using the velocity Verlet algorithm with a time step of 1 fs. A snapshot of the m40t20 system at 200 ns is shown in Figure 1b.

In order to verify that similar structures are obtained in different simulations, we analyzed the density, the radial distribution function

(RDF), the torsion angle distribution, and the orientational ordering parameter. The density variation with respect to the simulation time is shown in the top panel of Figure 2. After 4 ns high-temperature

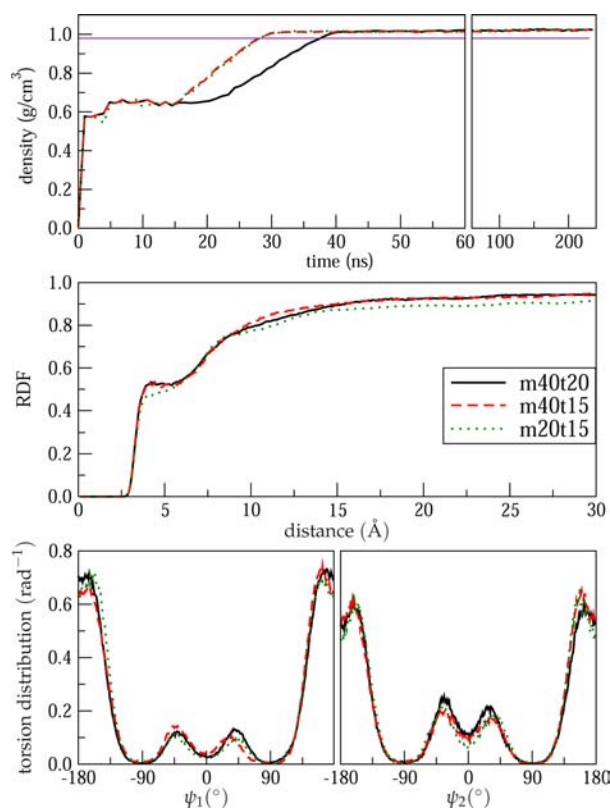


Figure 2. Top panel: density as a function of simulation time. The purple line denotes the experimental density of 0.98 g/cm³.⁴⁴ Middle panel: interchain radial distribution function of backbone C_{sp}² atoms. Bottom panel: torsion angle distribution for ψ_1 and ψ_2 (defined in Figure 1a).

equilibration, all systems reach the density of 0.64 g/cm³ until the simulated annealing from 1000 to 300 K is initiated at 15 or 20 ns. It can be seen that the three systems converge to the same density of 1.02 g/cm³ already at the end of the annealing procedure, a value close to the experimental density of 0.98 g/cm³.⁴⁴ The same final density of an amorphous structure was also found starting from an initial configuration where all chains are perfectly elongated and aligning along the same directions. However, the final simulation box was too anisotropic (245 × 64 × 17 Å), and to exclude possible spurious effects, we do not present those results here.

The middle panel of Figure 2 shows the interchain RDF of the backbone C_{sp}² atoms. The bottom panel of Figure 2 shows the torsion angle distribution of two different angles along the chain backbone. The RDF and the torsion angle distribution were averaged over 100 snapshots with 10 ps interval prior to 200 ns. It can be seen that both the RDF and the torsion angle distribution have converged to the same functions for the three systems. The very broad torsional angle distribution, consistent with the inspection of the MD snapshots, is expected to have a major role in the electronic structure as we will demonstrate in the next section.

To investigate the anisotropy of the systems, we considered the orientational ordering parameter S , which is defined as the largest eigenvalue of the order tensor $Q_{\alpha\beta}$.⁴⁵

$$Q_{\alpha\beta} = \frac{1}{N_c} \sum_i \left\{ \frac{3}{2} u_{i\alpha} u_{i\beta} - \frac{1}{2} \delta_{\alpha\beta} \right\} \quad (1)$$

where $\delta_{\alpha\beta}$ is the Kronecker delta function, u_i is the unit vector defining the orientation of each polymer (parallel to the line connecting the

first and last atoms), and N_c is the total number of chains. The smaller the value of S (always between 0 and 1), the more isotropic the system. We found that different systems converge to a value of S around 0.2. Considering the finite-size effect that only 16 chains are involved in the simulations, the final states are nearly isotropic.

For the subsequent analysis of the electronic structure, it is important to establish if the global shape of the individual chains changes during the hundreds of nanoseconds simulation. We have therefore considered two shape parameters for all chains in the simulations. First, we considered the gyration radius defined as⁴⁶

$$R_g = \frac{1}{n} \sum_{k=1}^M (\mathbf{r}_k - \bar{\mathbf{r}}) \quad (2)$$

where \mathbf{r}_k is the monomer position, $\bar{\mathbf{r}}$ is the mean position of all monomers, and M is the total number of monomers in each chain. We have also considered the chain anisotropy A_c defined as²⁰

$$A_c = \frac{3S_c}{2 + S_c} \quad (3)$$

where S_c is the orientational ordering parameter for an individual chain, defined as the orientation of parameter S (see eq 1) but with the unit vector indicating the orientation of each monomer. A_c is close to 1 for perfectly straight polymers and close to zero if there is no special direction in space for the orientation of the polymer chain.

Figure 3 illustrates the time dependence of the individual polymer chains for the m40t20 system. The range of gyration radii and anisotropies is very broad, indicating that the simulation box contains both globular chains ($R_g \sim 15$ Å) and rather elongated chains ($R_g \sim 50$ Å). These properties of the polymers oscillate very rapidly (indicating a very good equilibration) during the high-temperature simulation, while they remain essentially unchanged for hundreds of nanoseconds at room temperature. We learn from this analysis that if the aim is to study the “average” electronic structure of a bulk polymer, it is better to build more starting models than run extremely long simulations. This analysis also illustrates that it is not possible to confirm that the final structure of the simulation has reached its thermodynamical equilibrium or how far it is from a fully equilibrated structure as the time scale for the diffusion of the chains in the melt is orders of magnitude larger than the time scale that can be explored with atomistic MD. On the other hand, having verified that different simulations converge to structures with very similar characteristics (density, radial and dihedral distribution functions, various order parameters), we can be confident to have generated a rather plausible model from the amorphous phase that should be sufficient to explore the relation between polymer conformation and electronic structure.

The computation of the electronic structure of a very disordered amorphous bulk polymer is extremely demanding considering that polymer chains in our MD simulations have ~1000 atoms in the 20 monomer system and ~2000 atoms in the 40 monomer system. Therefore, it is necessary to adopt some approximations. First, the side group $-\text{OC}_3\text{H}_7$ of each chain will be replaced by the $-\text{OCH}_3$ group in order to speed up the calculation without altering the nature of the conduction and valence band states.⁴⁷ This simplification is physically sound since the main features of the electronic structure largely depend on backbone structures.⁴⁸ Second, we will initially assume that the electronic coupling of an individual chain with its surrounding chains is negligible, and we therefore calculate the electronic structure of each individual chain separately. The validity of this assumption will be explicitly verified below, by computing the electronic coupling between individual chains.

The B3LYP functional^{49,50} was employed for the electronic structure calculations of the individual chains. To reproduce the electrostatic environment of each polymer, point charges are added in the position of the atoms close to the polymer chain of interest but belonging to other chains. The values of the point charges were the same used for the force field (optimized to reproduce the short-range electrostatic interaction). To avoid including an unbalanced number of point charges, the monomers of the surrounding chains within 10 Å from any atoms on the chain are identified first. The point charges for

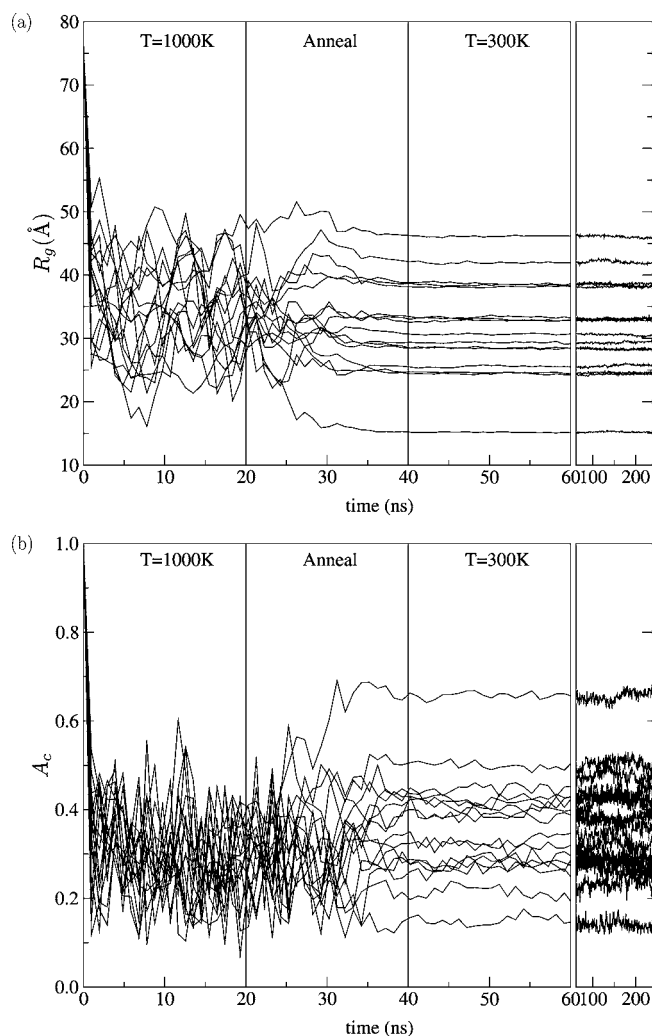


Figure 3. (a) Gyration radius and (b) chain anisotropy for the 16 individual polymer chains of the m40t20 system along the trajectory.

all atoms on these monomers (including the full side chains) are then added. The total charge on a monomer is null, and so the interactions that are switched on at the cutoff distance are of the dipole–dipole type, decreasing as the cube of the distance. This cutoff scheme is similar in spirit to that used in fast multipole methods,⁵¹ and we have verified that the energy difference between occupied orbitals changes by less than 5% by increasing the cutoff to 25 Å.

The electronic structure is analyzed in terms of the DOS and the localization length of the one-electron states.^{6,52,53} The DOS per chain per monomer $\rho_{c,i}(E)$ is defined as

$$\rho_{c,i}(E) = \sum_m \delta(E - E_i^{(m)})/M \quad (4)$$

where $E_i^{(m)}$ is the energy of the molecular orbital m for chain i , and M is the number of monomers per chain. The bulk DOS of a polymer system can then be calculated assuming the interchain coupling is negligible as

$$\rho_b(E) = \sum_{i=1}^{N_c} \rho_{c,i}(E)/N_c \quad (5)$$

where N_c is the total number of chains. To avoid confusion with other approaches, we note that the DOS in this work is defined for one-electron states entirely filled or empty below and above the band gap, respectively. According to such definition, the valence band states do not include the effect of polarization that takes place when they are populated by a hole. Calculations of the DOS that incorporate these

effects are possible when the localization of the one-electron states is known in advance as in small molecule systems.⁵⁴ Consistently with the definition used here, the interaction with the environment is due to the interaction with fixed point charges and excludes polarization effects. Such effects may be incorporated at a later stage when the charge transport is modeled but are outside the scope of this work.

Denoting $C_i^{(m)}$ as the coefficient for atomic orbital i for molecular orbital m , the normalization of the orbitals implies $\sum_{ij} C_i^{(m)} S_{ij} C_j^{(m)} = 1$, where S_{ij} is the overlap matrix of the basis set. If a system is partitioned into monomers, the weight of molecular orbital m on a given monomer k can be defined as

$$P_k^{(m)} = \sum_{\substack{i \text{ on monomer } k \\ j \text{ on all monomers}}} C_i^{(m)} S_{ij} C_j^{(m)} \quad (6)$$

and we have $\sum_k P_k^{(m)} = 1$, where the sum goes over all the monomers for each chain. Indicating with \mathbf{r}_k the position of the center of mass of monomer k , the centroid of the molecular orbital m can be defined as $\mathbf{R}^{(m)} = \sum_{k=1}^M \mathbf{r}_k P_k^{(m)}$, and the localization length for molecular orbital m can then be defined as

$$L^{(m)} = 2 \left(\sum_{k=1}^M |\mathbf{r}_k - \mathbf{R}^{(m)}|^2 P_k^{(m)} \right)^{1/2} \quad (7)$$

An energy-dependent localization length for chain i can be defined as

$$L_{c,i}(E) = \frac{\sum_m L^{(m)} \delta(E - E^{(m)})}{\sum_m \delta(E - E^{(m)})} \quad (8)$$

and the bulk localization length of a polymer system can then be calculated as

$$L_b(E) = \sum_{i=1}^{N_c} L_{c,i}(E)/N_c \quad (9)$$

For numerical calculation of eq 4 and eq 8, $\delta(E - E^{(m)})$ was approximated with a normalized Gaussian of standard deviation $\sigma = 0.1$ eV.

RESULTS AND DISCUSSION

The m20t15 structure at 200 ns was chosen for a preliminary comparison between the results obtained using the 3-21G and 6-31G* basis sets. Figure 4 shows that the difference is very little while using different basis sets for $\rho_{c,i}(E)$ and $L_{c,i}(E)$. The localization length and DOS have a pronounced chain-to-chain variation but change only marginally when a different basis set is used. Since the variability between chains is much larger than the possible inaccuracy of the small 3-21G basis set, for a given amount of computational time, it is best to evaluate more snapshots (conformations) with a lower basis set accuracy. For this reason, 3-21G calculations will be used to analyze more snapshots of the larger system containing 40 monomers (8 snapshots separated by 25 ns of simulated trajectory time).

Figure 5 shows the bulk (i.e., averaged over all chains) DOS and the localization length averaged over eight snapshots. The computed band gap is 2.0 eV, close to the experimental value of 2.2 eV,⁵⁵ and insensitive to the length of the polymer chains used in the simulation. This observation represents the first strong indication that the length of the polymer is sufficient to reproduce the bulk electronic properties of the material.

The bottom panels of Figure 4 and Figure 5 show that states near the gap are more localized. The orbitals relevant for p-type transport are within 1 eV from the valence band edge (there are approximately 10 orbitals in this range for the 40 monomer model). The localization length around the valence band edge is about 20 Å, which is about the length of 4 monomers, and it

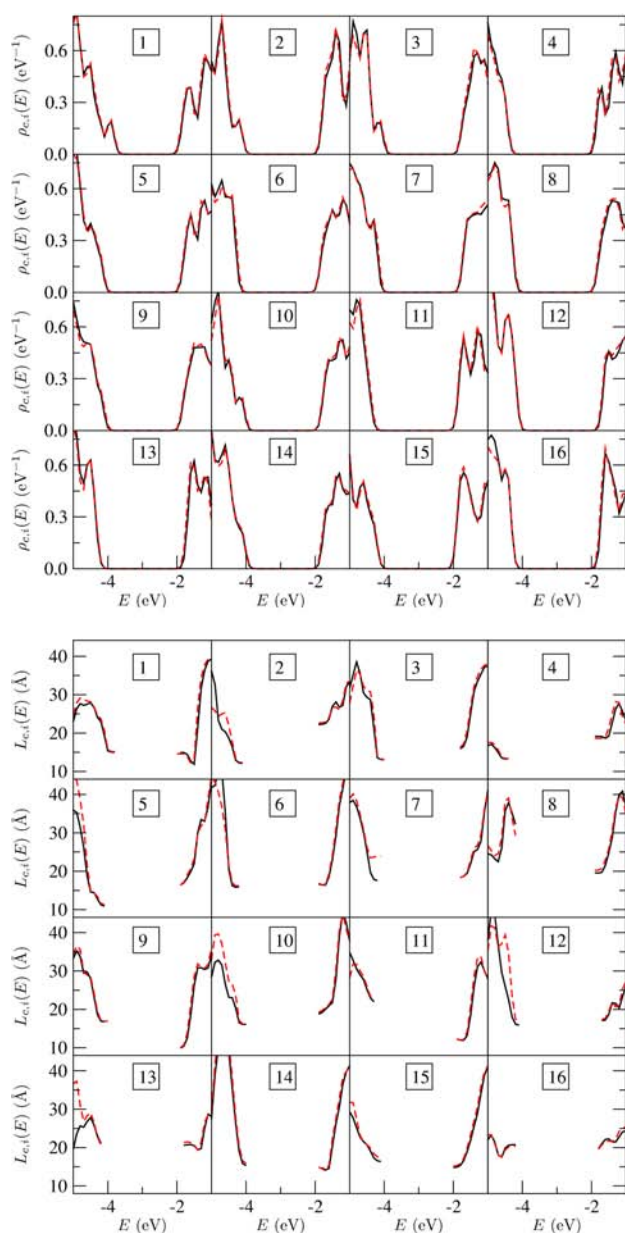


Figure 4. Density of states (top panel) and localization length (bottom panel) for the 16 individual chains of the m20t15 system at 200 ns. The solid black line denotes the results using 3-21G basis set, and the dashed red line denotes the results using 6-31G* basis set.

increases up to ~ 35 Å, which is about the length of 6 monomers. The localization length is significantly smaller than the length of the straight polymer (130 or 260 Å for the chain of 20 or 40 monomers) and smaller than the gyration diameter (twice the gyration radius) in the range of [40 Å, 100 Å] as shown in Figure 3a. This indicates that the orbital localization should not be too affected by the size of the model studied. The bottom panel of Figure 5 shows that the localization length within the first ~ 1 eV for the chain with the 40 monomers is slightly larger than the chain with 20 monomers, indicating that the 20 monomer chains have localization characteristics not yet similar to that of the infinite chain. On the other hand, the localization length increases only by 10% upon doubling the polymer length; that is, the localization character for the 40 monomer chain is likely to be very similar to that of a very long polymer.

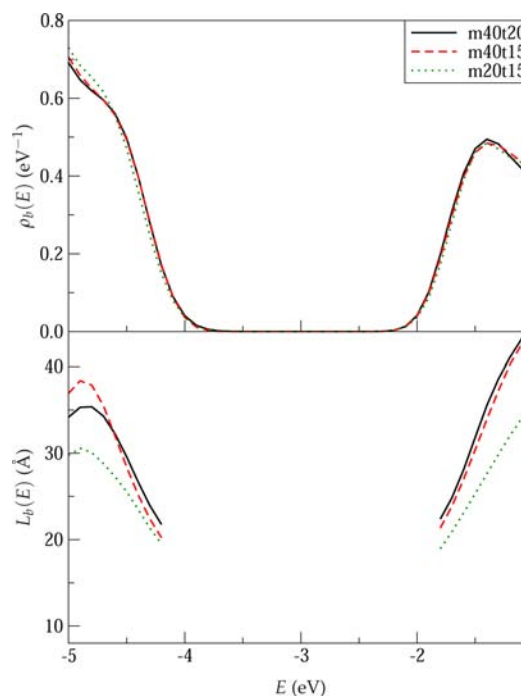


Figure 5. Top panel: bulk density of states. Bottom panel: bulk localization length for different systems by averaging eight snapshots from 25 to 200 ns every 25 ns.

It should be kept in mind, however, that simulations of polymers with molecular weight of 5–10 kDa, like the one performed here, cannot capture the morphological changes that occur in a polymer at much higher molecular weight, where chain entanglement and aggregation of the polymer is known to take place. The convergence of the electronic properties observed above is therefore valid as long as the change of molecular weight does not affect the polymer morphology. Evidence of such morphological changes for molecular weight between 100 and 2800 kDa is given for example in ref 56.

The disorder in the system is primarily caused by the chain configuration with a contribution of the electrostatic disorder that we have simulated using background point charges. We can quantitatively evaluate the importance of electrostatic disorder by repeating the calculation of the DOS without background charges. Figure 6 shows that the shape of $\rho_b(E)$ is not altered significantly when the background charges are removed for all three systems. The conduction band is not much affected, while the valence band is shifted by ~ 0.15 eV to higher energy when background charges are included. The average results of Figure 6 hide the effect of background charges on the individual orbitals. In a test reported in the Supporting Information, we show that the localization and position of the HOMO orbital in 20 monomer chains is modified in 2 cases out of 16 as a result of the inclusion of the point charges. The inclusion of the background charges is therefore necessary for our calculations but probably does not alter the essential transport properties. The relatively small effect of electrostatic disorder is possibly not a general feature of all semiconducting polymers. Polymers with a larger dipole moment in the monomer (like P3HT studied in ref 33, or copolymers with donor–acceptor characteristics) may display a greater role of electrostatic disorder. Moreover, if the electronic conjugation is weaker, like in many donor–acceptor copolymers, the effect of electrostatic disorder is not necessarily weaker than the disorder due to the

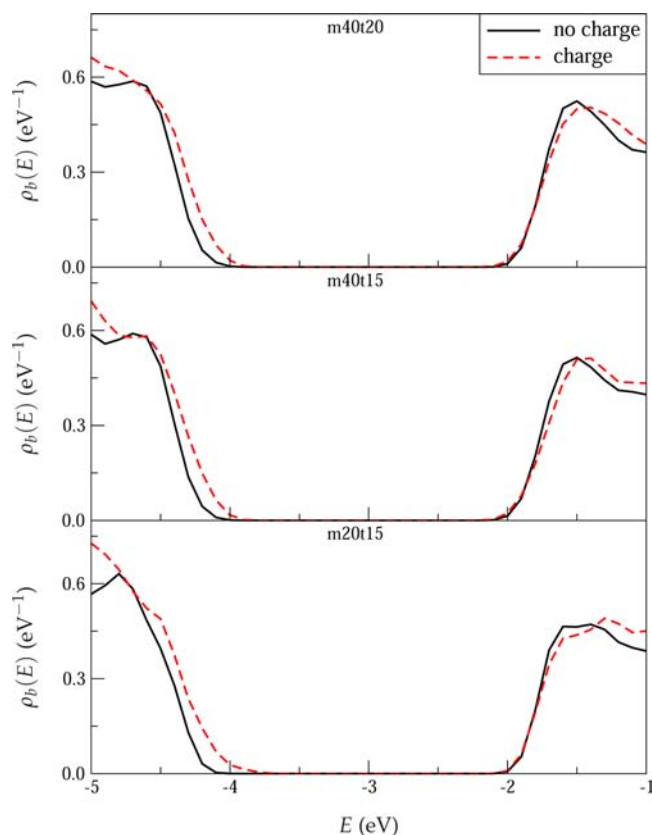


Figure 6. Comparison of bulk DOS with and without background charges for three systems at 200 ns.

chain configuration. In any case, the proposed methodology should be able to capture these effects when applied to different polymers.

By computing the electronic structure for individual chains, we have neglected up to this point the orbital coupling between chains. This was evaluated for the m20t15 structure at 200 ns (with $-\text{OC}_8\text{H}_7$ replaced by $-\text{OCH}_3$ for consistency with the electronic structure calculation). The electronic coupling between a range of the highest occupied orbitals (from HOMO-9 to HOMO) for any pair of chain was computed from⁵⁷

$$V_{ij}^{\alpha,\beta} = \langle \phi_\alpha^0 | \hat{F}^0 | \phi_\beta^0 \rangle \quad (10)$$

where ϕ_α^0 and ϕ_β^0 are unperturbed valence band orbitals localized on chains i and j , respectively. \hat{F}^0 is the Fock operator of the system of the two chains using the unperturbed density matrix. The images of the pair of chains in the periodic system were chosen to have minimal distance between their mid-atoms. The 10×10 couplings between the 10 highest occupied orbitals of the individual chains have been computed, and the maximum of these couplings V_{ij}^{\max} is chosen to represent the significance of the interchain coupling.

We report in Figure 7a the distribution of V_{ij}^{\max} excluding the pairs of chains whose closest interatomic distance was larger than 4 Å (to exclude pairs of chains for which V_{ij}^{\max} is negligible and not very informative). These calculations show that most coupling values are less than 20 meV; the coupling value around 70 meV occurs twice, and the largest value of 90 meV occurs only once. Therefore, the influence of other chains on the electronic structure of one chain can be neglected, and the

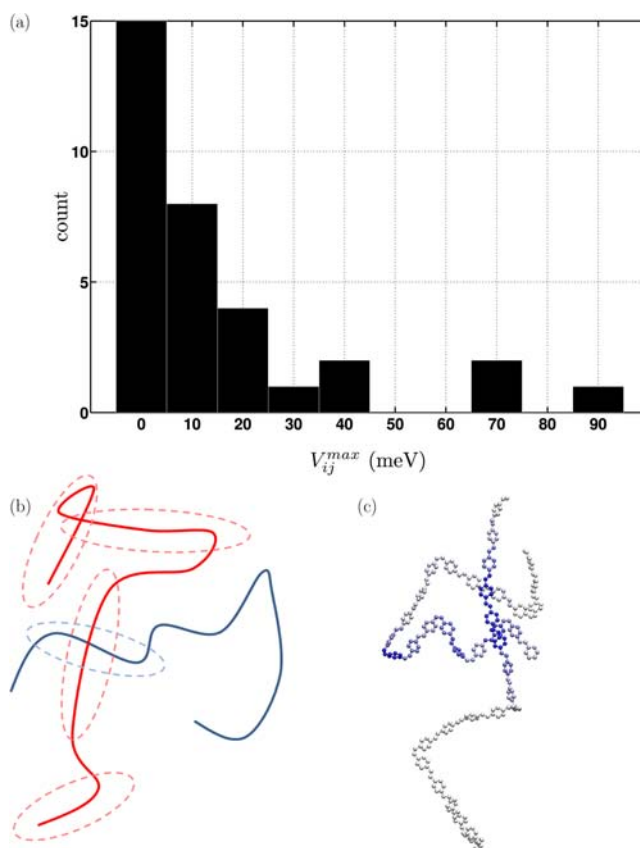


Figure 7. (a) Distribution of V_{ij}^{\max} . (b) Sketch of orbitals in two close chains. (c) Two chains with the largest coupling value of 90 meV. The HOMO is colored in blue, with its orbital density represented by the depth of blue color. Only the carbon backbone atoms are shown for each chain.

DOS reported on the basis of single-chain calculations is representative of the DOS in the bulk. The very limited electronic coupling between chains is easy to rationalize. When two chains are in contact, most of the orbitals will be localized away from the point of contact (see Figure 7b), and for the orbital close to the point of contact, the overlap will be minimal. It is not surprising that the largest coupling is observed for two very delocalized orbitals belonging to two very close chains (Figure 7c).

To evaluate the likelihood that orbitals across different chains are hybridized, we can consider that, for coupling around 10 meV, some hybridization will occur if the orbitals are closer in energy than approximately 50 meV. Considering that the 10 highest occupied orbitals included in the calculation of the data in Figure 7 have energies spanning approximately 1 eV, the probability of an orbital to hybridize is somewhat around 5% (or lower if we focus on orbitals on the band edge where the DOS is lower).

The computational schemes that we have validated mirrors the electronic structure and the nature of charge transport in these polymers. The greatest role in determining the electronic structure is the single-chain conformation, a zero-th order effect that we have described through an accurate variational procedure (the DFT calculation). The interchain coupling is clearly a small perturbation with respect to the effect of the single-chain conformation as it is appropriately evaluated within a perturbative scheme. This aspect hints to the possibility that the mechanisms of intrachain transport and interchain transport

should be discussed with clearly distinct quantum dynamics methodologies.

The gyration radius and chain anisotropy of individual polymer chains shown in Figure 3 reach a stationary value after 50 ns at room temperature. However, slight variations of the chain conformation could occur due to thermal motion, as seen in the top part of Figure 8. Somewhat surprisingly, these

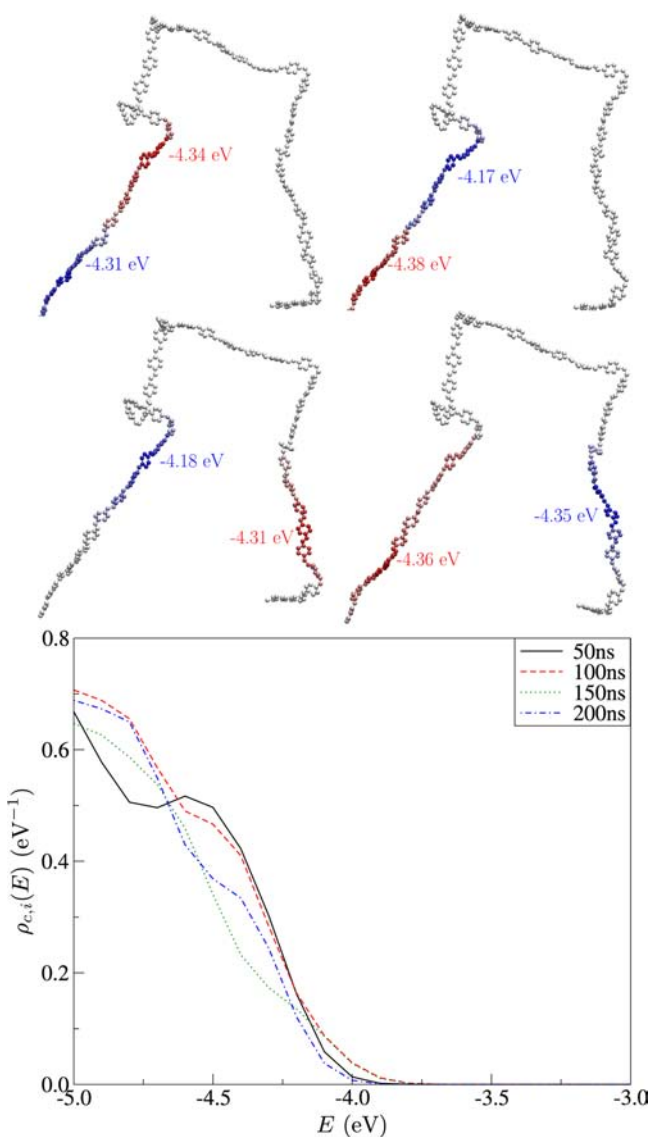


Figure 8. Variation of DOS at different room temperature snapshots for a chain of the m40t20 system. The associated backbone structures are shown in the top part in the sequences of 50, 100, 150, and 200 ns. HOMO-1 orbitals are colored in red, and HOMO orbitals are colored in blue, with its orbital density represented by the color depth. The energies for HOMO-1 and HOMO are also shown.

apparently modest changes of conformation lead to significant changes in the electronic structure of the chain, as shown in the DOS in Figure 8 for a representative chain. This could be reflected in the positions of HOMO orbitals illustrated in the top part of Figure 8. In practice, the energy of the highest occupied orbitals fluctuates slowly (~ 0.2 eV), and their energy ordering can be altered in the time scale of tens of nanoseconds. For example, the order of HOMO-1 and HOMO orbitals is inverted between 50 and 100 ns and

between 150 and 200 ns. A consequence of this observation is that it is desirable to compute the DOS from atomistic structure at an interval of several tens of nanoseconds to provide a more accurate average as what we have done in Figure 5. It should be also noted that these structural changes are too slow with respect to the charge dynamics, unlike what is observed in liquid-crystalline semiconductors,⁵⁸ and the disorder in these materials can be considered static.⁵⁹

Chain folding and chain nonplanarity have often been used to characterize the defects in disordered systems,^{6,19} and it is therefore reasonable to look for correlations between the occurrence of these defects and the localization of the frontier orbital. Having access to a large number of conformations and orbital evaluations, we can study these connections more systematically.

The chain folding is caused by so-called tetrahedral defects^{60,61} illustrated in Figure 9 and found when two

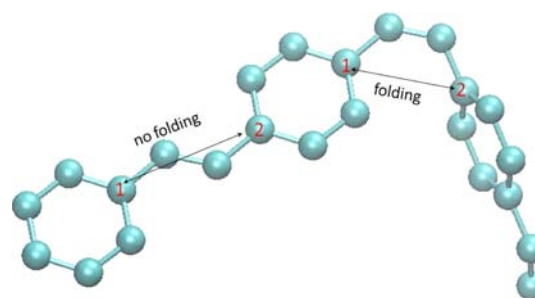


Figure 9. Sketch of chain folding within a MEH-PPV single chain. Only the backbone carbon atoms are shown. The chain folding arises from a tetrahedral defect which can be characterized by a shorter distance between type 1 and type 2 atoms.

consecutive aromatic rings are particularly close. Considering the two carbon atoms in consecutive aromatic rings separated by a vinylene unit (labeled as 1 and 2 in Figure 9), the distance d between them can be used to monitor the presence of a defect. The equilibrium distance between atom type 1 and atom type 2 of the next monomer is approximately 3.9 Å. Thus $\Delta_k^{(d)} = |d - 3.9|$ can represent the degree of chain folding at monomer k if d is the distance between type 1 and type 2 atoms.

Here our analysis is focused on HOMO orbitals, and this analysis can be straightforwardly extended to other orbitals. A folding degree of a polymer chain in the region where the HOMO is localized can be defined as

$$\lambda_f^{\text{HOMO}} = \sum_{k=1}^M \Delta_k^{(d)} P_k \quad (11)$$

where P_k is the HOMO orbital density on monomer k (defined in eq 6) and M is the total number of monomers per chain. The average folding degree of a chain can be defined as

$$\lambda_f^{\text{chain}} = \sum_{k=1}^M \Delta_k^{(d)} / M \quad (12)$$

It was proposed that high-energy valence orbitals (the traps for the holes) are localized in the region of the polymer that are locally more planar.⁶ This was verified for semicrystalline P3HT with different levels of regioregularity.⁶ To verify if the same conclusion is true for the amorphous PPV derivative, we define a torsion angle displacement from planarity as

$$\Delta_k^{(\psi)} = \min\{|\psi|, 180 - |\psi|\} \quad (13)$$

The MEH-PPV chain nonplanarity mainly arises from two torsion angles ψ_1 and ψ_2 , as shown in Figure 1a. Then the nonplanarity degree for monomer k can be defined as

$$\bar{\Delta}_k^{(\psi)} = (\Delta_k^{(\psi_1)} + \Delta_k^{(\psi_2)})/2 \quad (14)$$

Similarly, the nonplanarity degree in the region of the HOMO can be defined as

$$\lambda_p^{\text{HOMO}} = \sum_{k=1}^M \bar{\Delta}_k^{(\psi)} P_k \quad (15)$$

and the average nonplanarity per chain can be defined as

$$\lambda_p^{\text{chain}} = \sum_{k=1}^M \bar{\Delta}_k^{(\psi)} / M \quad (16)$$

When the distribution of λ_f^{HOMO} and λ_f^{chain} values obtained repeating the calculations on many chains is compared, it is possible to establish the correlation between the HOMO positions and the folding positions. If there is no correlation between the position of the HOMO and the geometric feature of chain folding, the distributions of λ_f^{HOMO} and λ_f^{chain} would overlap. We find instead (Figure 10) that λ_f^{HOMO} is distributed in the range of [0 Å, 0.35 Å] with its peak around 0.05 Å, and λ_f^{chain} is distributed in the range of [0.1 Å, 0.35 Å] with its peak around 0.25 Å. It means that the HOMO is preferentially localized away from the folding region, as indicated in literature and exemplified in Figure 11a. However, the overlap between these two distributions also implies that exceptions exist and are

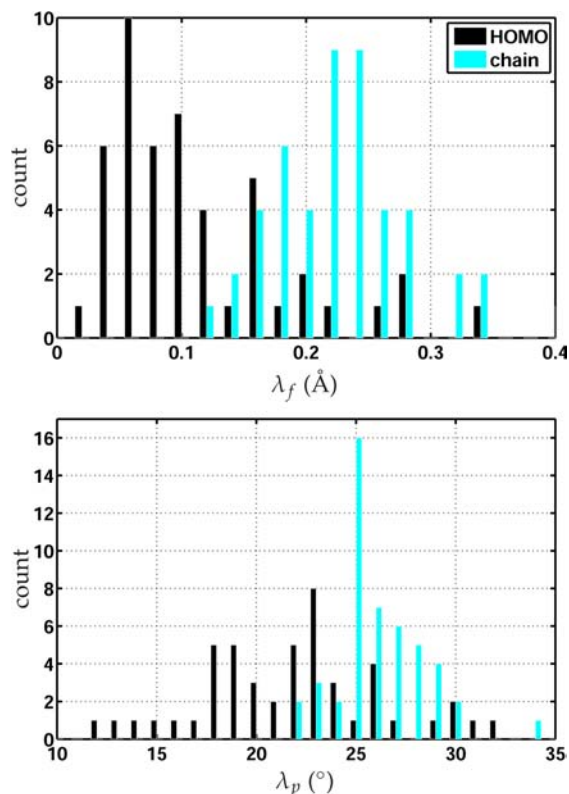


Figure 10. Histogram distribution of chain folding in the top panel and nonplanarity degree in the bottom panel for 48 chains of three systems at 200 ns.

not rare, as shown for example in Figure 11b. It has been generally assumed that the folding positions can break the polymer chain into fragments that can be considered the “units of transport” where the charge carrier can be localized.¹⁵ Our results show that this simplification cannot be used in general to devise a theory of transport in amorphous polymers and highlight the importance of carrying out explicit quantum chemical calculations before formulating phenomenological theories.

A similar phenomenon has been observed in the bottom panel of Figure 10 regarding the relation between HOMO localization of and the planarity of the chain. The distribution of λ_f^{chain} is shifted to lower angles with respect to the distribution of λ_f^{HOMO} , indicating that the HOMO is found more preferably in planar regions. However, the overlap between the two distributions implies that it is relatively common to find HOMO orbitals located in a nonplanar region (e.g., as in Figure 11d). For an amorphous system, there is a large degree of nonplanarity as implied by the broad torsion angle distribution in the bottom panel of Figure 2. Consequently, it should not be too surprising that few highest occupied orbitals are localized in nonplanar regions.

CONCLUSION

We have employed classical molecular dynamics simulations to build several models of the amorphous semiconductor MEH-PPV, and we have computed the electronic structure of the models to obtain information relevant for the charge transport properties of this material. The main methodological innovation consists of the calculation of the electronic structure of the isolated chains, surrounded by point charges that mimic the actual electrostatic environment, followed by the calculation of the orbital coupling between chains. A balanced set of approximations was determined in order to provide the best possible evaluation of the density of states of the system for a given amount of computational resources. The electronic structure of very large models of bulk polymers provides many essential elements for the modeling of charge transport in these materials. The main findings can be outlined as follows:

(i) We have verified, by explicit calculation, that the electronic structure is largely determined by the conformational disorder of the individual chains. The effect of electrostatic disorder is modest (in PPV), and the effect of electronic coupling between chains is even less important. These findings, easy to rationalize on the basis of the available data, suggest that the transport mechanism along the chain and across chains may follow different mechanisms, as the nature of the interaction between states localized within the same chain or in different chains is different.

(ii) We have verified that the model used is sufficiently large to reproduce the density of states and the localization length of realistic polymer chains, which are typically much longer than the chain used in any computable model. The localization length of the relevant orbitals is energy-dependent, unlike what is normally assumed in variable range hopping methods.

(iii) We analyzed the nature of the highest orbitals of the valence band, that is, the traps for the electron holes in this p-type semiconductor, in terms of their lifetime with respect to the dynamics of the polymer. The energy of these states fluctuates very slowly, approximately tenths of electronvolts within 10–50 ns, making them “static traps” from the point of view of the charge carrier. The overall shape of the polymer

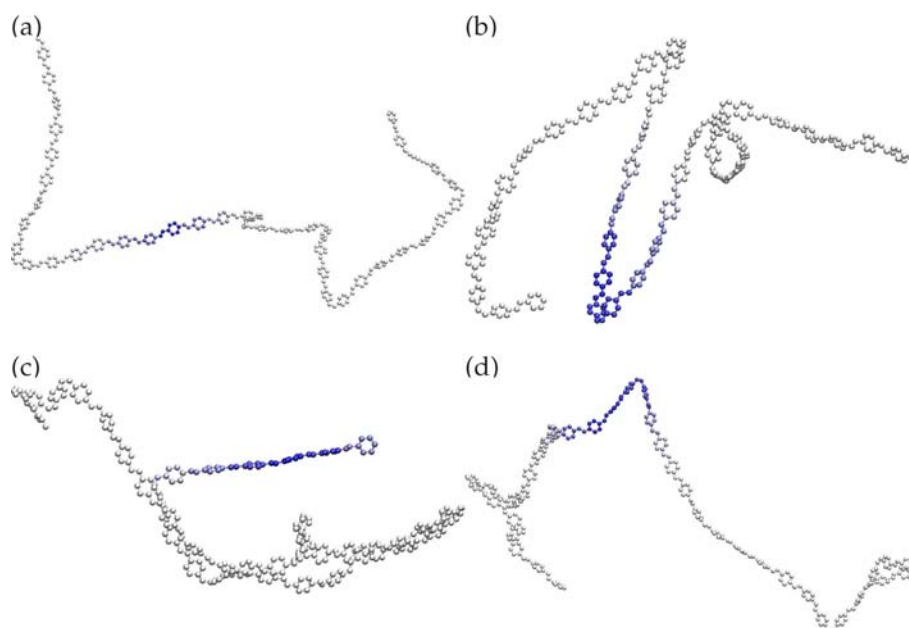


Figure 11. HOMO of representative chains. The HOMO is colored in blue, with its orbital density represented by the depth of the blue color. Only the carbon backbone atoms are shown for each chain. (a) HOMO far away from folding position; (b) HOMO around folding position; (c) HOMO in a planar region; (d) HOMO in a nonplanar region.

chain is essentially unchanged for at least hundreds of nanoseconds.

(iv) We tested the idea that the highest orbitals of the valence band may be localized in regions which are relatively planar and far from polymer “folding”. Although we have found evidence of correlation between planarity and localization of the highest valence band orbitals, the correlation is moderate and many exceptions are observed. A phenomenological model of transport should not therefore rely on some arbitrary partitions of the system in conjugated fragments.

This work has been designed to inform the construction of a model of transport in amorphous polymers. However, some of the features identified above (variable localization length and difference between intrachain and interchain transport) do not allow a direct transfer of parameters from this atomistic calculation into an existing transport models,¹ but instead, they suggest that some more general model should be built to correctly account for realistic electronic structure.⁵ The four points listed above among the key findings of the paper are rather insensitive to the approximations made to reach them. In particular, if the actual structure of low molecular mass PPV is slightly more ordered as a result of very slow equilibration, this will not affect the relation between conformation and electronic structure. Among the additional information to be included in a transport model beyond what is presented here, we should mention the charge stabilization due to nuclear and electronic polarization effects. Both are dependent on the localization length of the charge carrier state, and the results of this work should form a suitable starting point for their computational investigation.

Finally, it should be remembered that this model, like any atomistic model, cannot account for extrinsic defects that are found in all materials from ultrapure crystal to amorphous solids and may determine the mobility at low charge concentration through an additional exponential tail of defect states.^{62,63}

■ ASSOCIATED CONTENT

📄 Supporting Information

Force field parametrization and validation; test on the effect of the background point charges on orbital localization. This material is available free of charge via the Internet at <http://pubs.acs.org>.

■ AUTHOR INFORMATION

Corresponding Author

a.troisi@warwick.ac.uk

Notes

The authors declare no competing financial interest.

■ ACKNOWLEDGMENTS

The work is supported by the European Research Council. Computational resources for this work were provided by the Centre for Scientific Computing, University of Warwick, and the UK national supercomputing service, HECToR. The authors wish to thank David L. Cheung for his help on molecular dynamics simulations. We also would like to thank Rocco Fornari and Tao Liu for helpful comments on the manuscript.

■ REFERENCES

- (1) Tessler, N.; Preezant, Y.; Rappaport, N.; Roichman, Y. *Adv. Mater.* **2009**, *21*, 2741–2761.
- (2) Mendels, D.; Tessler, N. *J. Phys. Chem. C* **2013**, *117*, 3287–3293.
- (3) Salleo, A.; Kline, R. J.; DeLongchamp, D. M.; Chabiny, M. L. *Adv. Mater.* **2010**, *22*, 3812–3838.
- (4) Zaumseil, J.; Sirringhaus, H. *Chem. Rev.* **2007**, *107*, 1296–1323.
- (5) Rivnay, J.; Mannsfeld, S. C. B.; Miller, C. E.; Salleo, A.; Toney, M. F. *Chem. Rev.* **2012**, *112*, 5488–5519.
- (6) McMahon, D. P.; Cheung, D. L.; Goris, L.; Dacuña, J.; Salleo, A.; Troisi, A. *J. Phys. Chem. C* **2011**, *115*, 19386–19393.
- (7) McCulloch, I.; Heeney, M.; Bailey, C.; Genevicius, K.; MacDonald, I.; Shkunov, M.; Sparrowe, D.; Tierney, S.; Wagner, R.; Zhang, W.; Chabiny, M. L.; Kline, R. J.; McGehee, M. D.; Toney, M. F. *Nat. Mater.* **2006**, *5*, 328–333.

- (8) McCulloch, I.; Ashraf, R. S.; Biniak, L.; Bronstein, H.; Combe, C.; Donaghey, J. E.; James, D. I.; Nielsen, C. B.; Schroeder, B. C.; Zhang, W. *Acc. Chem. Res.* **2012**, *45*, 714–722.
- (9) Nielsen, C. B.; Turbiez, M.; McCulloch, I. *Adv. Mater.* **2013**, *25*, 1859–1880.
- (10) Mott, N. F.; Davis, E. A. *Electronic Processes in Non-crystalline Materials*, 2nd ed.; Clarendon Press: Oxford, U.K., 2012.
- (11) Mott, N. F. *Philos. Mag.* **1969**, *19*, 835–852.
- (12) Tessler, N.; Roichman, Y. *Org. Electron.* **2005**, *6*, 200–210.
- (13) Padmanaban, G.; Ramakrishnan, S. *J. Am. Chem. Soc.* **2000**, *122*, 2244–2251.
- (14) Hennebicq, E.; Deleener, C.; Brédas, J.-L.; Scholes, G. D.; Beljonne, D. *J. Chem. Phys.* **2006**, *125*, 054901-16.
- (15) Collini, E.; Scholes, G. D. *Science* **2009**, *323*, 369–373.
- (16) Sun, H.; Mumby, S. J.; Maple, J. R.; Hagler, A. T. *J. Am. Chem. Soc.* **1994**, *116*, 2978–2987.
- (17) De Leener, C.; Hennebicq, E.; Sancho-Garcia, J.-C.; Beljonne, D. *J. Phys. Chem. B* **2009**, *113*, 1311–1322.
- (18) Kumar, P.; Mehta, A.; Mahurin, S. M.; Dai, S.; Dadmun, M. D.; Sumpter, B. G.; Barnes, M. D. *Macromolecules* **2004**, *37*, 6132–6140.
- (19) Hu, D.; Yu, J.; Wong, K.; Bagchi, B.; Rossky, P. J.; Barbara, P. F. *Nature* **2000**, *405*, 1030–1033.
- (20) Adachi, T.; Brazard, J.; Chokshi, P.; Bolinger, J. C.; Ganesan, V.; Barbara, P. F. *J. Phys. Chem. C* **2010**, *114*, 20896–20902.
- (21) Huang, D. M.; Moulé, A. J.; Faller, R. *Fluid Phase Equilib.* **2011**, *302*, 21–25.
- (22) Huang, D. M.; Faller, R.; Do, K.; Moulé, A. J. *J. Chem. Theory Comput.* **2010**, *6*, 526–537.
- (23) Marcon, V.; Raos, G. *J. Phys. Chem. B* **2004**, *108*, 18053–18064.
- (24) Marcon, V.; van der Vegt, N.; Wegner, G.; Raos, G. *J. Phys. Chem. B* **2006**, *110*, 5253–5261.
- (25) Bounos, G.; Ghosh, S.; Lee, A. K.; Plunkett, K. N.; DuBay, K. H.; Bolinger, J. C.; Zhang, R.; Friesner, R. A.; Nuckolls, C.; Reichman, D. R.; Barbara, P. F. *J. Am. Chem. Soc.* **2011**, *133*, 10155–10160.
- (26) DuBay, K. H.; Hall, M. L.; Hughes, T. F.; Wu, C.; Reichman, D. R.; Friesner, R. A. *J. Chem. Theory Comput.* **2012**, *8*, 4556–4569.
- (27) McMahan, D. P.; Cheung, D. L.; Troisi, A. *J. Phys. Chem. Lett.* **2011**, *2*, 2737–2741.
- (28) McMahan, D. P.; Troisi, A. *Chem. Phys. Lett.* **2009**, *480*, 210–214.
- (29) Vukmirović, N.; Wang, L.-W. *Nano Lett.* **2009**, *9*, 3996–4000.
- (30) Vukmirović, N.; Wang, L.-W. *J. Chem. Phys.* **2011**, *134*, 094119-8.
- (31) Kitaura, K.; Ikeo, E.; Asada, T.; Nakano, T.; Uebayasi, M. *Chem. Phys. Lett.* **1999**, *313*, 701–706.
- (32) Vukmirović, N.; Ponseca, C. S.; Němec, H.; Yartsev, A.; Sundström, V. *J. Phys. Chem. C* **2012**, *116*, 19665–19672.
- (33) Vukmirović, N.; Wang, L.-W. *J. Phys. Chem. B* **2011**, *115*, 1792–1797.
- (34) Barford, W.; Boczarow, I.; Wharram, T. *J. Phys. Chem. A* **2011**, *115*, 9111–9119.
- (35) Barford, W. *J. Phys. Chem. A* **2013**, *117*, 2665–2671.
- (36) Sterpone, F.; Rossky, P. J. *J. Phys. Chem. B* **2008**, *112*, 4983–4993.
- (37) Fukuzawa, K.; Komeiji, Y.; Mochizuki, Y.; Kato, A.; Nakano, T.; Tanaka, S. *J. Comput. Chem.* **2006**, *27*, 948–960.
- (38) Seijo, L.; Barandiaran, Z. *J. Chem. Phys.* **2004**, *121*, 6698–6709.
- (39) Allinger, N. L.; Yuh, Y. H.; Liü, J. H. *J. Am. Chem. Soc.* **1989**, *111*, 8551–8566.
- (40) Allinger, N. L.; Li, F.; Yan, L.; Tai, J. C. *J. Comput. Chem.* **1990**, *11*, 868–895.
- (41) Sprague, J. T.; Tai, J. C.; Yuh, Y.; Allinger, N. L. *J. Comput. Chem.* **1987**, *8*, 581–603.
- (42) Moreno, M.; Casalegno, M.; Raos, G.; Meille, S. V.; Po, R. *J. Phys. Chem. B* **2010**, *114*, 1591–1602.
- (43) Jorgensen, W. L.; Tirado-Rives, J. *J. Am. Chem. Soc.* **1988**, *110*, 1657–1666.
- (44) Ou-Yang, W.-C.; Chang, C.-S.; Chen, H.-L.; Tsao, C.-S.; Peng, K.-Y.; Chen, S.-A.; Han, C. C. *Phys. Rev. E* **2005**, *72*, 031802.
- (45) Cheung, D. L.; Troisi, A. *Phys. Chem. Chem. Phys.* **2009**, *11*, 2105–2112.
- (46) Ravve, A. *Principles of Polymer Chemistry*, 3rd ed.; Springer: New York, 2012.
- (47) Nayyar, I. H.; Batista, E. R.; Tretiak, S.; Saxena, A.; Smith, D. L.; Martin, R. L. *J. Phys. Chem. Lett.* **2011**, *2*, 566–571.
- (48) Wong, K. F.; Skaf, M. S.; Yang, C.-Y.; Rossky, P. J.; Bagchi, B.; Hu, D.; Yu, J.; Barbara, P. F. *J. Phys. Chem. B* **2001**, *105*, 6103–6107.
- (49) Becke, A. D. *J. Chem. Phys.* **1993**, *98*, 5648–5652.
- (50) Lee, C.; Yang, W.; Parr, R. G. *Phys. Rev. B* **1988**, *37*, 785–789.
- (51) Kurzak, J.; Pettit, B. M. *Mol. Simul.* **2006**, *32*, 775–790.
- (52) Troisi, A.; Orlandi, G. *Phys. Rev. Lett.* **2006**, *96*, 086601.
- (53) Baez, L. A. Ph.D. Thesis, Cornell University, New York, 1996.
- (54) May, F.; Baumeier, B.; Lennartz, C.; Andrienko, D. *Phys. Rev. Lett.* **2012**, *109*, 136401.
- (55) Jørgensen, M.; Krebs, F. *Polym. Bull.* **2003**, *51*, 23–30.
- (56) Shaked, S.; Tal, S.; Roichman, Y.; Razin, A.; Xiao, S.; Eichen, Y.; Tessler, N. *Adv. Mater.* **2003**, *15*, 913–916.
- (57) Troisi, A.; Orlandi, G. *J. Phys. Chem. A* **2006**, *110*, 4065–4070.
- (58) Troisi, A.; Cheung, D. L.; Andrienko, D. *Phys. Rev. Lett.* **2009**, *102*, 116602.
- (59) McMahan, D. P.; Troisi, A. *ChemPhysChem* **2010**, *11*, 2067–2074.
- (60) Sumpter, B. G.; Kumar, P.; Mehta, A.; Barnes, M. D.; Shelton, W. A.; Harrison, R. J. *J. Phys. Chem. B* **2005**, *109*, 7671–7685.
- (61) Padmanabhan, V. Ph.D. Thesis, Columbia University, New York, 2009.
- (62) Tanase, C.; Blom, P. W. M.; de Leeuw, D. M.; Meijer, E. J. *Phys. Status Solidi A* **2004**, *201*, 1236–1245.
- (63) Pernstich, K. P.; Rössner, B.; Batlogg, B. *Nat. Mater.* **2008**, *7*, 321–325.